Simultaneous Segmentation of Bone Regions Using Multiple-Level Threshold

Huang C. Y.[1], Lee P. Y.[2], Lai J. Y.[3], Luo L. J.[4], Tsai Y. C.[5] and Lin S.C.[6]

[1]National Central University, Taoyuan, ROC, 94340304@cc.ncu.edu.tw
[2]Show Chwan Memorial Hospital, Changhua, ROC, hary7700@yahoo.com.tw
[3]National Central University, Taoyuan, ROC, jylai@ncu.edu.tw
[4]Pou Yuen Technology Ltd., Changhua , ROC, 963203069@cc.ncu.edu.tw
[5]Pou Yuen Technology Ltd., Changhua , ROC, s1343011@cc.ncu.edu.tw
[6]National Taiwan University of Science and Technology, Taipei, ROC, xyz@mail.ntust.edu.tw

ABSTRACT

Conventional approaches to segmenting skeletal structures include extracting 2D contour profiles on the 2D image domain and performing 3D region growing to acquire the 3D bone region directly. However, as far as multiple pieces of bones segmentation are concerned, these methods are not accurate or efficient enough as each bone must be processed one by one. The purpose of this study is to present a method for multiple bones segmentation. A seed regions generation algorithm is proposed to automatically generate an initial region on each bone of interest. The seed regions are then expanded iteratively. In this process, simultaneous region growing is employed to control the moving speed of the fronts, which can reduce the occurrence of overflow. An investigation of the initial threshold and target threshold is also conducted and appropriate methods to optimize the values are provided. Moreover, five cases of lower limbs are employed to demonstrate the feasibility of the proposed method.

Keywords: 3D bone reconstruction, contour detection, multiple-level threshold.
DOI: 10.3722/cadaps.2011.269-288

1   INTRODUCTION

3D visualization techniques such as volume rendering and maximum/minimum intensity projection can easily be employed to display skeletal structures. The examples shown in Figure 1 represent the isosurface of several skeletal structures by a volume rendering technique. Although such data seem to be visually pleasing, no surface boundary can be accessed from such a representation because such data only represent the mapping of 3D data onto the 2D viewing plane. The primary shortcoming of this representation is that the joint area may easily be obstructed and can never be observed in any view. Moreover, it is impossible to display and manipulate an individual bone owing to the limitations

of this representation. To overcome such a problem, segmentation of the bones of interest is necessary.

The 3D skeletal structures have many applications, including visualization, diagnosis, implant design, surgical planning and simulation. Although several 3D methods exist for vessels, brains, organs and skeletal structures, segmentation is still the major bottleneck because clinical applications require a fast, robust and efficient approach for real-time display and operation. In CT images, the contrast between the bones and the surrounding tissues is generally high. However, the overlapping intensity distribution between the bones and the surrounding tissues makes it difficult to segment the bones accurately and completely.
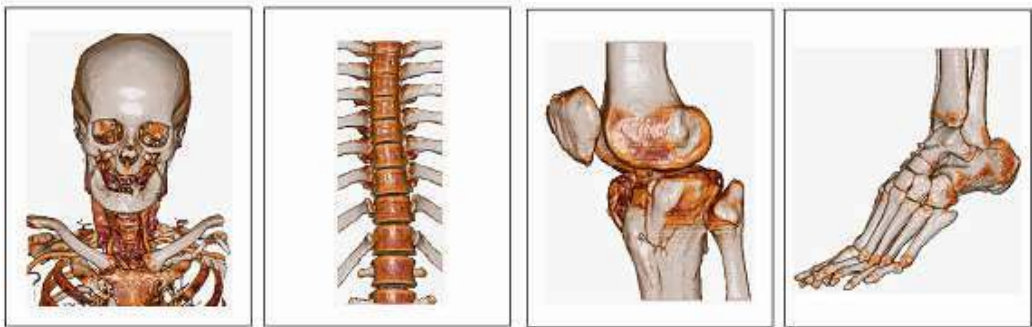

Fig. 1: Isosurface representation of skeletal structures by a volume rendering.

Bone segmentation approaches can be classified into three kinds: interactive, semi-automatic and fully automatic. The interactive approach is typically implemented on 2D images, in which the contour of the bone of interest is detected or drawn slice by slice. This method is time consuming and error-prone. On the contrary, the fully automatic approach requires less manual effort and is generally the best method. However, it is the most difficult approach due to the inherent complexity and variety of medical images. Most available approaches are still semi-automatic as they can cope with the accuracy as well as the completeness of the bone model.

3D region growing is a common method for bone segmentation. Starting from a seed point, the region is expanded along the six-neighborhoods of each voxel on a front in accordance with a certain criteria. All new boundary voxels are added to the front and the expansion is continued until all voxels on the front have been checked. Constant thresholding is typically employed for the growing of an iso-surface. It can easily yield a bone model for any of the examples shown in Figure 1. The model may not be very accurate, yet, it is good enough for the purpose of visualization. However, as far as the accuracy and completeness of the model is concerned, constant thresholding is still not good enough. Various methods have been proposed to determine the threshold value for the constant thresholding technique. Histogram-based approaches have been used to evaluate the intensity distribution of entire images and determine an optimized threshold in terms of cross entropy ([1],[2]), cumulative moments [3], moving threshold [4] and variance minimization through dilations [5]. These methods have been referred to as global thresholding as the threshold is determined in terms of the global histogram of the images. They have worked satisfactorily when there is significant difference in gray values between the background and the object. For actual CT images, however, the intensity distribution near the transition of the bones and the surrounding issues may not be uniform, resulting in difficulty in deciding an appropriate threshold for all slices of images. Multiple thresholding techniques in terms of cross entropy [6] and Ostu's cumulative moments ([7],[8]) have also been presented to deal with multi-object images. These methods, however, are more suitable for histograms with several distinct peaks.

Another type of region growing involves providing rules to determine the similarity between the tested voxel and the growing region locally. Seeded region growing [9] (SRG) employs the mean and standard deviation of the growing region to determine the similarity of the tested pixel and the growing region; while unseeded region growing [10] (URG) emphasizes automatic determination of seeded points, with the same growing criteria as those shown in SRG. Justice et al. [11] modified the SRG algorithm by extending the search to 3D and generating the seeds automatically through the use of thresholds. Revol-Muller et al. [5] provided several assessment functions in terms of boundary criteria and region criteria to determine the optimal homogeneity criterion for 3D region growing. Sekiguchi and Sano [12] employed two criteria in accordance with the difference between adjacent pixels and the difference between the tested pixel and the seed point, respectively, to determine the homogeneity criterion. A leakage removal procedure was also implemented to extract and remove leakage regions automatically. Hojjatoleslami and Kittler [13] defined an average contrast measure in terms of two boundaries: current boundary, which was the set of pixels adjacent to the current region, and internal boundary, which was the boundary produced by the set of connected outermost pixels of the current region. They claimed that region growing produced increasing average contrast measure values as long as high intensity pixels were continuously included. Pohle and Toennies [14] conducted adaptive region growing in which an upper bound and a lower bound of the thresholds in terms of the mean and standard deviation of the neighborhoods around the seed point were defined. Two runs of region growing were presented. The first run was employed for evaluating homogeneity parameters, while the second run was employed for extracting the region.

As for the segmentation of skeletal structures, Kwan et al. [15] proposed an approach composed of gap pixel identification, fragment filtering and gap extension and widening for automatic extraction of bone boundaries on 2D images, especially for narrow gaps. A fuzzy multilevel thresholding algorithm was employed to deal with the overlapping of the intensity distribution of different tissues on the histogram. Kang et al. [16] proposed a highly automated method for the segmentation of 3D bones. They proposed 3D region growing in terms of local adaptive thresholds, in which the intensity distribution near the intersection of bones and surrounding tissues were fitted into Gaussian functions, by which the upper bound and lower bound of the thresholds were determined for growing. This was followed by procedures to correct for remaining boundary discontinuities and a subsequent anatomically oriented boundary adjustment using local values of cortical bone density.

Wang et al. [17] presented a method to validate the segmentation of CT images and improved the accuracy and efficiency of the subsequent registration of the three-dimensional reconstructed surfaces. The similarity or coherency of neighboring contours was measured by comparing statistical properties. Descoteaux et al. [18] proposed a multi-scale sheet enhancement measure for paranasal sinus bone segmentation by means of local shape information obtained from an eigenvalue decomposition of the Hessian matrix. Conventional segmentation by thresholding was not suitable for thin bones as it resulted in holes and diffuse boundaries due to partial volume effects and noise in CT datasets. Zoroofi et al. [19] proposed several techniques for segmenting the pelvis and the femur, in particular, the acetabulum and the femoral head in the hip joint. Their method was primarily divided into three steps: preprocessing, histogram based thresholding and binary and morphological operations. Their study provided a detailed description of the algorithm for each of the steps. Testi et al. [20] focused on the implementation and validation of a border-tracing method for the extraction of endosteal canal contours. The result of this method was compared with those obtained by the manual method and the threshold-based technique. Westin et al. [21] proposed a new solution to the problems caused by constant thresholding based on three-dimensional filtering techniques. The fundamental concept of their approach was to design an adaptive filtering algorithm to emphasize structures of interest in CT images to make segmentation of bones easier.

In the segmentation of multiple pieces of bones, the most difficult problem is the separation of the bones near the joint area. Ideally, adjacent bones are separated by a thin layer of soft tissue and the intensity of the soft tissue is different from that of its adjacent bones such that a clear boundary

can be recognized. However, in real CT images, the boundaries of adjacent bones may become vague when the transition between the soft tissue and the bone is not clear enough. This may even result in the leakage of the gray values from one region to its neighboring region. The gray levels on such adjacent regions are so similar that none of the above threshold-determining techniques can deal with such a problem robustly. In addition, when multiple pieces of bones are concerned, the seed points are conventionally assigned manually. Even if they are determined automatically, the available algorithms are usually not robust enough to deal with all kinds of situations on the CT images. Therefore, it is necessary to develop an integrated procedure that can achieve the segmentation of all kinds of bones.

The aim of this study is to present a method for segmenting skeletal structures from two-dimensional slices of CT images. An integrated procedure is proposed to make sure that all bone regions can be segmented accurately, completely and efficiently. The proposed method includes automatic seed region definition, iterative region growing, as well as region re-combination and re-segmentation. In conventional region growing in which no restriction is made, it is difficult to separate different bones accurately because multiple regions of points may be combined together owing to the overflow problem. Iterative region growing by means of an intermediate target threshold is proposed to prevent such a problem. This ensures that all fronts can proceed to the common boundary at the same speed. Moreover, an optimized method for determining the initial threshold and target threshold is provided. Five cases of lower limbs are employed to demonstrate the feasibility of the proposed method.

2 MATERIAL AND METHODS

2.1 Overall Method

The input is a sequence of CT slices, which store digital images and communications in DICOM format. Each slice of the CT images has a fixed size of 512 x 512 pixels and a gray value of 12 bits. The image data must first be converted into volume data for easier processing. The volume data are essentially three-dimensional matrices recording the gray value of each voxel (a pixel in 3D images), where the first dimension represents the index of the slices, while the second and third dimensions represent the indices of the pixels on a slice. The overall process of the proposed method for segmenting skeletal structures can be divided into the following three stages:

- **Determination of thresholds:** two thresholds must be determined according to the proposed method: initial threshold T_i and target threshold T_t. The initial threshold is employed to assign seed points as well as to generate initial regions; while the target threshold is served as the terminal condition of the growing of each seed region.

- **Iterative 3D region growing:** The goal is to assign a seed point on each skeletal structure, and then grow an individual region for each of the seed points. All regions are grown iteratively, in which specific constraints are implemented to avoid the occurrence of overflow. Iterative region growing essentially includes two steps: automatic seed region generation and simultaneous multiple region growing. In particular, an intermediate target threshold is introduced to control the moving speed of the fronts such that they can reach the common boundary at the same time. With the proposed algorithm, all adjacent bones can be separated and grown individually.

- **Region re-combination and re-segmentation:** for complex or large skeletal structures with vague boundaries, some of the regions may not be segmented properly. Post-processing including a region re-combination and a region re-segmentation is employed to ensure that all regions can be segmented accurately and completely. The post-processing algorithm is essentially very simple in operation and can achieve the task efficiently.

2.2 Determination of Threshold

Two thresholds must be determined in the proposed multiple-region growing algorithm: initial threshold T_i and target threshold T_t. The initial threshold T_i is employed for initial seed region growing. As the initial threshold T_i is increased, so is the number of seed regions obtained. This means that there is more chance to separate unclear boundaries. However, as T_i becomes larger, the risk of over segmentation is increased also. A user interface is provided such that whenever T_i is set, the seed regions are automatically displayed in real time. Figure 2 depicts an example near a knee joint for T_i=800, 600 and 400, where the numbers of seed regions obtained are 15, 12 and 5, respectively. It is noted that when a new T_i is set, the seed regions are evaluated and displayed immediately, enabling the user to determine the appropriate number of regions.
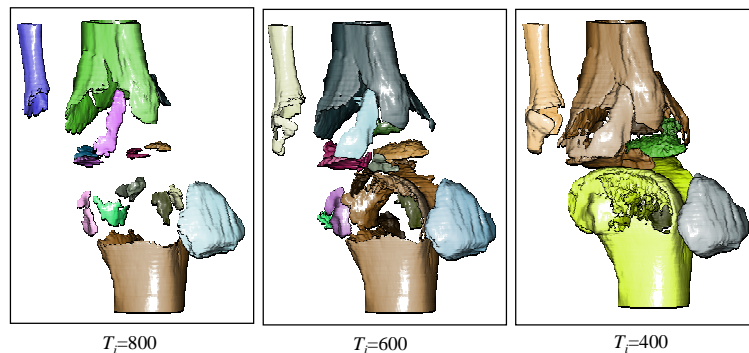

T_i=800 T_i=600 T_i=400

Fig. 2: Real-time display of seed regions in accordance with initial threshold T_i.

The target threshold T_t essentially determines the surface boundary of the final region. If T_t is too large, the growing may be stopped before it reaches the desired boundary, which may result in tiny regions or incomplete regions. On the contrary, if T_t is too small, the growing may overflow, e.g. several regions are wrongly connected or part of the surface boundary is over grown. An intensity distribution in accordance with the gray values of the entire images can be drawn to show the probability of each gray value, by which a rough threshold for the target bone can be determined. However, it is difficult to determine the cut-off threshold precisely as the lobes on the intensity plot are overlapped.

The transition of the gray values between the skeletal structure and its surrounding tissues is typically large, say over 1000. Thus, when the surface boundary is clear, the target threshold T_t can be determined easily. However, near the joint area where adjacent bones are separated by thin layers of soft tissue, the transition of the gray values is typically vague. Figure 3 indicates that there is a transition zone composed of several pixels between the target bone and its surrounding tissue on the gray-value plot. It is difficult to determine the target threshold as the shape of the transition zone and the number of pixels within it is changeable.
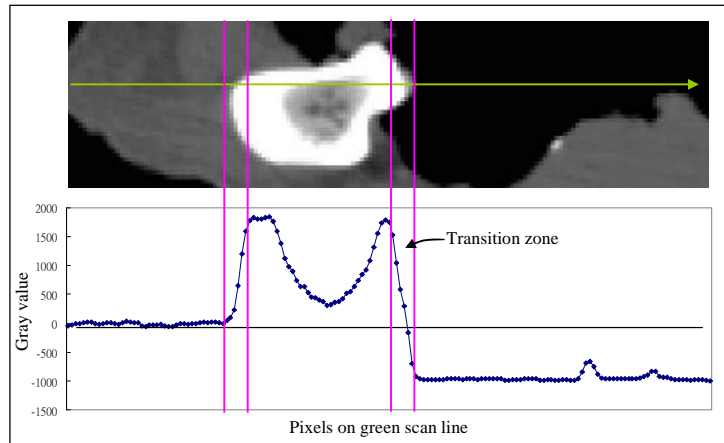
Fig. 3: The transition zone between a bone and its surrounding tissue is typically composed of several pixels.

When the boundary curve of two different tissues is available, the optimal threshold can be regarded as the average gray value of the pixels on the boundary curve [22]. The following expression can be employed to detect the edge boundary:

$$l(x, y) = \frac{\partial^2 f}{\partial x^2} + \frac{\partial^2 f}{\partial y^2} = 0 \tag{1}$$

$$\|\nabla f(x, y)\| > d \tag{2}$$

where $l(x,y)$ and $\|\nabla f(x, y)\|$ represent the Laplacian function and gradient magnitude function of $f(x,y)$, respectively, d is an allowable tolerance. Equation (1) denotes the zero-crossing of the second derivative of $f(x,y)$ and Eq. (2) denotes the peak magnitude of the first derivative of $f(x,y)$. The edge point corresponds to the status where the gradient magnitude reaches the maximum and the Laplacian function reaches zero. Since practical images are generally noised and imperfect, Eqs. (1) and (2) should be checked simultaneously to accurately detect the required edge boundary.

The Laplacian function is evaluated by means of eight neighborhoods of (x, y), while the gradient magnitude is evaluated by the Sobel edge detection mask. It is noted that to evaluate Eq. (1) on a 2D image, we must choose a pair of adjacent pixels that satisfy the following condition:

$$l(x_1, y_1) \cdot l(x_2, y_2) < 0 \tag{3}$$

where (x_1, y_1) and (x_2, y_2) denote two adjacent pixels in the region of interest. The pixel with the smaller gray value is chosen as the edge point.
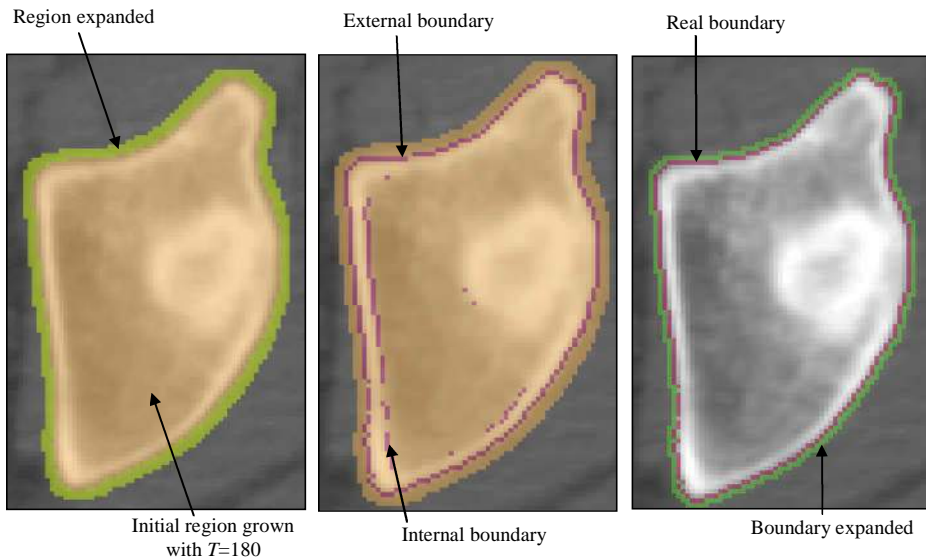
Fig. 4: Bone profile evaluation on a 2D image, (a) an expanded bone region is obtained, (b) edge points are obtained by Eq. (2) and (3), and (c) external boundary is extracted for evaluating optimal target threshold.

To fulfill the above concept of real CT images, a procedure is necessary to determine the boundary pixels as well as to choose the pixels for evaluating T_t. Figure 4 depicts the procedure for achieving this task. First, a threshold of 180 is employed to acquire a region (brown area in Figure 4(a)). This region is then expanded for two voxels to ensure that the skeletal structure is fully covered (green area in Figure 4(a)). Second, search the voxels within the brown and green regions to extract the voxels which satisfy Eqs. (2) and (3), shown as the purple voxels in Figure 4(b). It is noted that both the external and internal boundaries of the target bone are identified. Third, the internal boundary should be discarded as it distorts the target threshold. The brown region is shrunk until the purple boundary voxels are obtained, thus yielding the voxels of the external boundary. Once the voxels of the external boundary are obtained (purple voxels in Figure 4(c)), they are expanded outside for two voxels to yield a circle of voxels (green voxels in Figure 4(c)). The average gray value of these green voxels represents the optimized target threshold T_t for this 2D image. It is noted that T_t for different 2D images are usually different. Therefore, the above procedures should be implemented automatically.

2.3 Iterative 3D Region Growing

The proposed region growing algorithm is developed to grow multiple bones simultaneously, emphasizing accurate segmentation of the surfaces near the joint area. The proposed algorithm is essentially composed of the following two steps: (1) initial seed region growing and (2) simultaneous multiple region growing. Each of the two steps is discussed in detail below.

2.3.1 Seed Region Growing

This stage is made up of two procedures: automatic seed-point assignment and initial region growing. The seed-point assignment and initial region growing are performed in pairs. Whenever a seed point is assigned, it follows the growing of the initial region corresponding to that seed point. This ensures that all voxels of similar gray values are assigned to the same region. The following two rules are employed to check if a voxel is a seed point:

(1) The voxel hasn't been grown.

(2) Its gray value is larger than the initial threshold T_i.

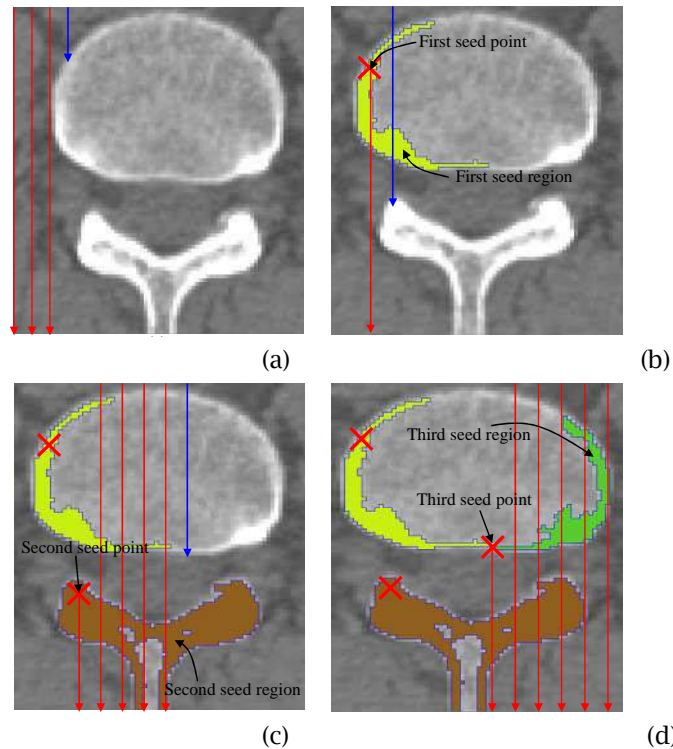If both rules are satisfied, the voxel is assigned as a seed point.

Fig. 5: Seed regions growing, (a) scanning the first seed point, (b) generating the first seed region, (c) generating the second seed point, and seed region, and (d) generating the last seed point and seed region.

Initial region growing is implemented as follows. Starting from the seed point, its six neighborhoods are tested in sequence to check if the above two rules are satisfied. Whenever a voxel is found, it is put into an array. Each voxel on the array is then tested to find its neighborhoods which satisfy the above two rules. All voxels found are also put into the array. Such a test is repeated until all voxels on the array have been tested, which finishes the growing. It is noted that a seed point may be located on a noised region. Therefore, a minimum number of voxels in a region is specified to avoid the generation of noised regions.

The overall procedure of seed region growing can be summarized as follows: Starting from the first voxel on the first slice of the images, the voxels on the images are tested sequentially. If a seed point is found, initial region growing is implemented. Once the region growing is finished, it is followed by the search of the next seed point. The voxel next to the current seed point is chosen as the starting point of the search, and each of the following voxels are checked. Whenever the above two rules are satisfied, the new seed point is found. The above process is continued until all voxels on the images have been tested.

Figure 5 depicts the search of the seed points and the growing of initial regions for a slice of CT images, where T_i=400 and T_t=180. As Figure 5(a) depicts, the search starts from the voxel on the upper left side and checks each voxel sequentially from left to right and top to bottom. The blue arrow indicates that the above two rules are satisfied, and hence it serves as the first seed point. The yellow region in Figure 5(b) is grown by means of the first seed point. The search is then continued to look for the second seed point, indicated by the blue arrow in Figure 5(b). The brown region in Figure 5(c) is grown by means of the second seed point. The third seed point is also indicated by the blue arrow in Figure 5(c). Finally, Figure 5(d) indicates that the green region is grown by means of the third seed point. The search is continued to the end of this image and no more seed points are found. Therefore, three seed regions are acquired.

2.3.2 Simultaneous Multiple Region Growing

Once all seed regions are acquired, they must be expanded in an appropriate sequence in order to yield the desired regions. When a region is expanded faster than its neighboring region, it may easily seize the voxels near the common boundary, and hence result in overflow. Figure 6 depicts three kinds of algorithms for expanding adjacent regions. In Figure 6(a), region A is expanded first, followed by region B. When there is a gap on the common boundary, region A easily crosses over the gap and occupies part of region B. In Figure 6(b), regions A and B are expanded in turn and each region is expanded for a width of one neighboring voxel each time. However, since the front of region A is initially close to the gap, region A still crosses over the gap and occupies part of region B. The method in Figure 6(c) is the modification of Figure 6(b). Basically, regions A and B are expanded in turn and for a width of one neighboring voxel as well. However, to avoid unequal speeds approaching the common boundary, an immediate target threshold T_m is employed to force both fronts to reach the same gray value during the expansion. As Figure 6(c) depicts, a decrement ΔT is specified to bring both fronts to reach the same gray value in each cycle of expansion. Therefore, even if region A is initially close to the gap, both regions reach the gap almost at the same iteration. We employ Figure 6(c) in the proposed algorithm.
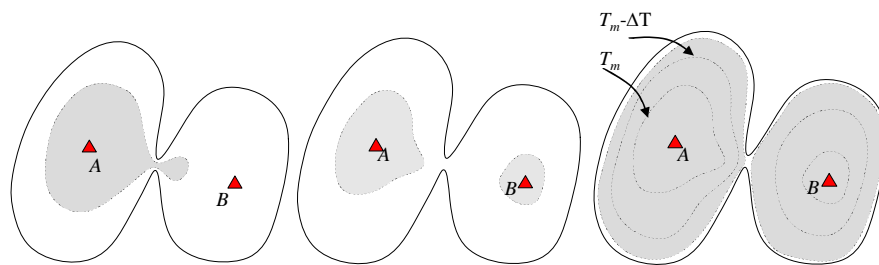

Fig. 6: Three kinds of region growing strategies, (a) region A and B are expanded separately, (b) regions A and B are expanded in turn, without restriction in speed on the fronts, and (c) regions A and B are expanded in turn, with restriction in speed on the fronts.

The flowchart of the proposed region growing algorithm in depicted in Figure 7. All the voxels on the region boundary are called a front. Initially, the gray values on all fronts are close to T_i. Iterative region growing is implemented to expand each region sequentially until the gray values of all fronts reach the target threshold T_t. In Figure 7, the iteration is essentially divided into two loops, where the inner loop expands each front in turn so that the gray values of all fronts can reach the intermediate threshold T_m, while the outer loop upgrades T_m until it reaches the final target threshold T_t. A detailed description of simultaneous multiple-region growing is given below.
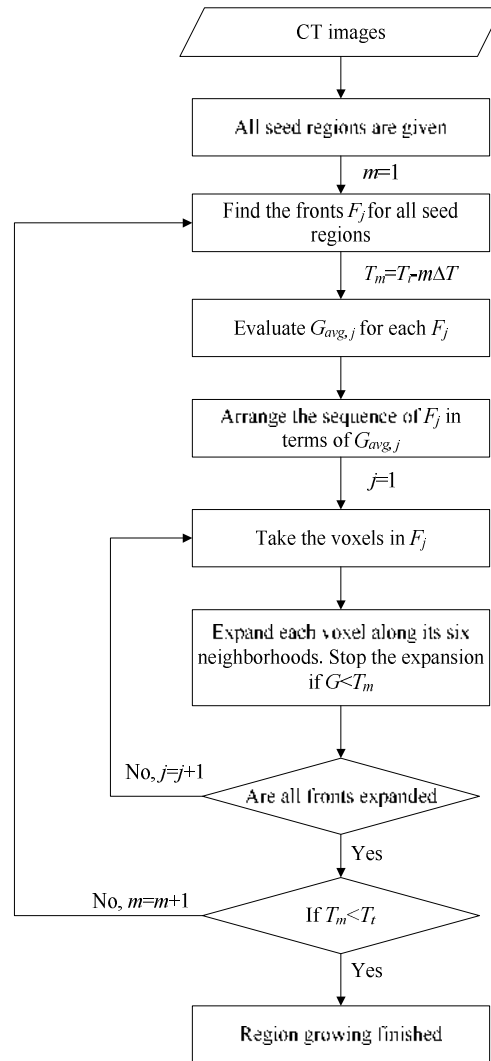
Fig. 7: Flowchart of simultaneous multiple regions growing.

First, the fronts F_i for all seed regions are found. Each front represents the collection of the boundary voxels of a seed region. Second, since the gray value of a bone is larger than its surrounding tissues, a front with larger gray value should be expanded first. Therefore, compute the average gray value of all the voxels on each front, termed $G_{avg,i}$, and then arrange the fronts in terms of $G_{avg,i}$ from maximum to minimum. The expansion of the fronts is carried out in accordance with such a sequence. Third, starting from the first front of the new sequence, each of the voxels on this front is expanded around its six neighborhoods. Assume that the gray value of its neighborhood is G. If $G \geq T_m$, where $T_m = T_i - m\Delta T$, the expansion can be carried out along this voxel. Otherwise, the expansion is stopped at this voxel. Whenever all voxels on a front have been tested, we then test the voxels of the next front. When all fronts have been tested, the inner loop of the iteration is completed. Fourth, the index m is increased by 1 to reduce the intermediate target threshold T_m for ΔT. If $T_m \geq T_t$, go back to the first step for the next cycle of expansion with an upgraded T_m. If $T_m < T_t$, stop the process.

Figure 8 depicts an example of a pelvis to illustrate the results of different region growing algorithms. In Figure 8(a), eight seed points are found automatically and each region is grown independently with a common target threshold of T_t=600. It is evident that all regions are not grown completely because T_t is too large. In Figure 8(b), T_t is reduced to 185 and all seed regions are grown one by one. The results show that all regions are completely grown as T_t is reduced from 600 to 185. However, overflow is observed in many regions as no rule is specified to restrict the growing near the joint area. In Figure 8(c), the iterative region growing is implemented, with T_i=600 and T_t=185. The results show that all regions are grown completely and no overflow is observed.
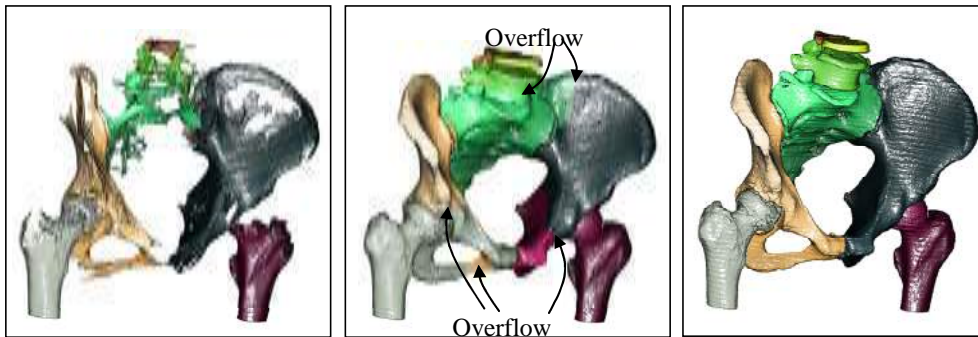

Fig. 8: Different region growing algorithms on a pelvis example, (a) all regions grown independently with T_t=600, (b) all regions grown independently with T_t=185, and (c) proposed iterative region growing with T_i=600 and T_t=185.
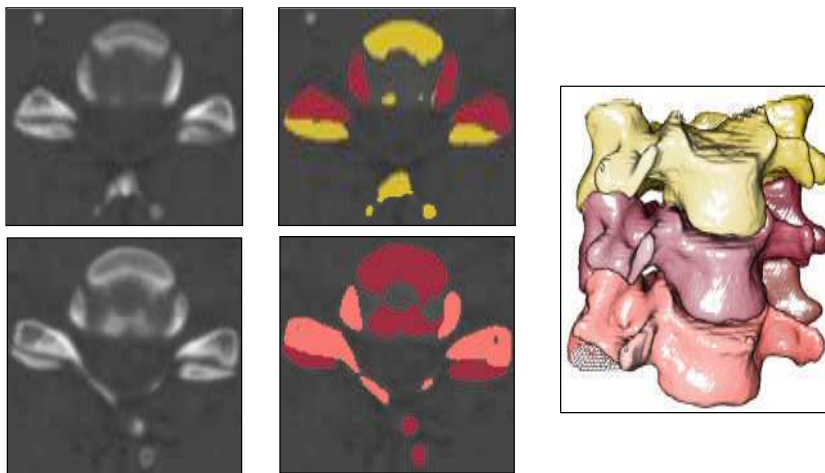

Fig. 9: Segmentation of unclear gray values near the joint area of a cervical vertebrae example, (a) two slices of the original images, (b) accurate segmentation of the shared boundary, and (c) 3D display of three separated bones.

To further demonstrate the capability of the proposed algorithm for bones with similar gray values in the joint area, two slices of the cervical vertebrae are discussed, in which the gray values at the common boundary are not very clear. Figure 9(a) depicts the original images, in which some of the boundaries cannot be distinguished visually. Figure 9(b) depicts the separated regions in different colors. The results show that the transition of adjacent bones is accurately identified. Figure 9(c)

depicts a 3D display of three separated bones, where each color represents an individual bone region. The results show that the joint areas of all bones are accurately separated and no overflow is observed.

2.4 Region Re-combination and Re-segmentation

It is unavoidable that some of the regions may wrongly be segmented. This is because the above-mentioned seed point assignment algorithm may not be robust enough to satisfy all kinds of CT images. To compensate for such a deficiency, a post-processing process including region re-combination and re-segmentation is developed. Region re-combination is employed to combine the regions which are over segmented, while region re-segmentation is employed to handle the under segmented cases.

2.4.1 Region Re-combination

Region re-combination is a process of combining separated regions into a single region, and can generally be implemented manually. However, when multiple regions are generated simultaneously, an automatic procedure is necessary to check for the possibility of re-combination. The following four coefficients are defined to judge the possibly of region re-combination:

(1) Region points N_i: number of voxels in region i.
(2) Adjacent points P_{ij}: number of voxels shared by two adjacent regions i and j.
(3) Adjacent faces F_{ij}: number of faces shared by two adjacent regions i and j.
(4) Average gradient in gray value k_{ij}: average difference in gray value per adjacent face for adjacent regions i and j. It is evaluated as follows: for each boundary voxel in region i, find its neighboring voxels in region j. For each pair of such voxels, evaluate the difference in gray values. Add all differences together and divide them by the adjacent faces F_{ij}, which yields k_{ij}.
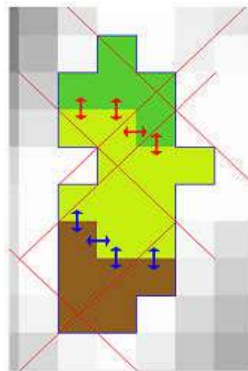

Fig. 10: An example showing the definition of four coefficients N_i, P_{ij}, F_{ij} and k_{ij}.

Figure 10 depicts an example showing the values of the above four coefficients. The four coefficients of the yellow region in Figure 10 are as follows: (1) N_i=10, (2) P_{ij} is 3 for both the green and brown regions, (3) F_{ij} is 4 for both the green and brown regions, and (4) for both the green and brown regions, the sum of the differences in gray values for the four pairs of the neighboring voxels is evaluated and k_{ij} is the sum divided by 4. Here N_i can be used to determine the size of a region; the ratio $s_{ij}=F_{ij}/P_{ij}$ can be used to judge the flatness of the boundary across adjacent regions. When s_{ij} is large, the boundary is less smooth. In general, when two adjacent regions belong to the same structure, s_{ij} should be small. The parameter k_{ij} is used to judge the variation of the gray values between two adjacent regions. When two regions belong to the same bone, k_{ij} should be small. Five rules are developed to judge whether or

not adjacent regions should be combined. If any of the following five rules are satisfied, the two regions can be combined into one region:

(1) $k_{ij} < 50$ and $F_{ij} > 100$ (judged by average difference in gray value per adjacent face)
(2) $k_{ij} < 80$ and $F_{ij} > 500$ (judged by average difference in gray value per adjacent face)
(3) $k_{ij} < 130$ and $s_{ij} < 1.5$ (judged by average difference in gray value per adjacent face and the flatness of the boundary)
(4) $s_{ij} < 1.8$ (judged by the flatness of the boundary)
(5) $P_{ij}/N_i > 0.1$ (judged by the ratio of the voxels on the boundary relative to total voxels in a region)

2.4.2   *Region Re-segmentation*

A global threshold T_i is not sufficient for segmenting all kinds of bones. Some of the bones may need a larger T_i for accurate extraction of the voxels near the common boundary. Others may need a smaller T_i to achieve the task. When a larger T_i is selected to fulfil the requirement of the former, it may result in over segmentation or incomplete growing for the latter. To deal with such a problem, it is suggested that the initial threshold T_i be less than 600 in multiple region growing. The regions which are not accurately separated can later be segmented by a region re-segmentation process.

The region re-segmentation algorithm is similar to the multiple regions growing algorithm, except that the region considered and the range of the initial threshold T_i is different. The region re-segmentation algorithm is only used for a particular region specified by the user. Therefore, the domain of the voxels searched is restricted to the region considered. This can easily be achieved when all voxels of the same region are marked with the same index in the data structure. Moreover, the initial threshold T_i is set to be larger than 600, say 800. This ensures that at least two seed regions can be obtained, and then grown into separated regions. The target threshold T_t is kept the same during the growing of the seed regions. Region re-segmentation can be implemented repeatedly until all regions are properly segmented.

3   RESULTS AND DISCUSSION

Five sets of CT images for the human lower limbs are employed to investigate the feasibility of the proposed method for multiple bone segmentation. Figure 11 shows the iso-surface display of the five lower limbs with a threshold of $T=180$. The threshold $T=180$ provides a quick display of the skeletal structures for visualization. However, not all surface boundaries are accurately described owing to the limitation of the constant threshold. Table 1 lists the DICOM information of the five cases, where the first three cases are from GE LightSpeed VCT, while the fourth and fifth cases are from SOMATOM Sensation 16 and Website OsiriX, respectively. The pixel spacing and slicing thickness for all five cases are between 0.66~0.832 mm and 1.0~1.4 mm, respectively. The slicing thickness is especially important as it may affect the accuracy of the segmentation results near the joints. The clearance between the femur and the tibia in the human lower limb is typically between 2~5 mm. The range 1.0~1.4 mm for the slicing thickness is less than the above clearance, and is regarded as acceptable. The aim here is to segment five major bones in each example, namely the ilium, femur, patella, tibia and fibula.

The initial threshold T_i and the target threshold T_t are two important parameters affecting the segmentation results and must be determined effectively. First, T_i is analyzed as follows. An initial region growing is performed by starting with a lower T_i to yield a region that combines all bones together. The same region growing is then repeated with T_i increased by 1 each time until a bone is separated. Take Figure 12 as an example. When T_i is increased from a lower value to 163, all regions are combined together (Figure 12(a)); when T_i is increased to 164, the patella is separated (the green object in Figure 12(b). Here $T_i=164$ is regarded as a critical threshold. As T_i is increased continuously, other bone regions are separated in sequence. Such a process is repeated until all five target bones are obtained. Table 2 lists all critical thresholds for five bones and five lower limbs in Figure 11, where the

left and right bones are also individually listed. The results indicate that the patella has the minimum critical threshold (average threshold=151), while the ilium has the maximum critical threshold (average threshold=402). The other three bones are in between (average threshold is between 284~291). Therefore, if all five bones must be separated individually, it would be better to set T_i=400; whereas, if four of them, except the ilium, must be separated, it would be better to set T_i=300. We perform similar tests for other skeletal structures, and the best ranges of T_i suggested are listed in Table 3. In general, one can choose the largest value of the corresponding range to ensure that a greater number of bones can be separated. Region re-combination can later be performed to combine the over segmented regions.
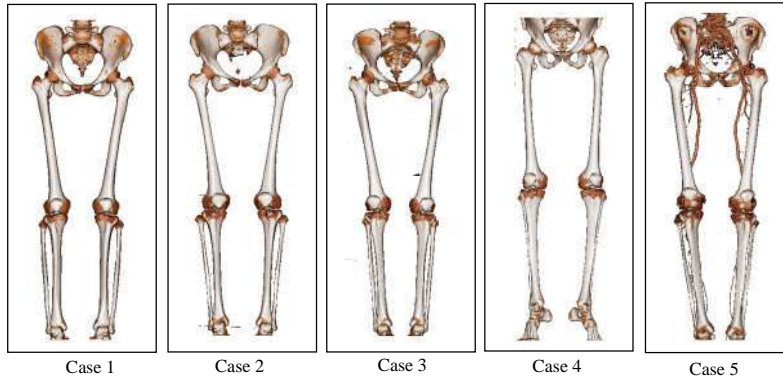

Case 1   Case 2   Case 3   Case 4   Case 5

Fig. 11: Iso-surface display of five lower limbs with a threshold T=180.

	Case 1	Case 2	Case 3	Case 4	Case 5
Machine	LightSpeed VCT			Sensation 16	From website OsiriX
Sex	Female	Female	Female	Male	Male
Age	18	20	36	30	No Info.
Pixel spacing (mm)	0.768	0.660	0.703	0.678	0.832
Slicing thickness (mm)	1.250	1.250	1.250	1.000	1.400

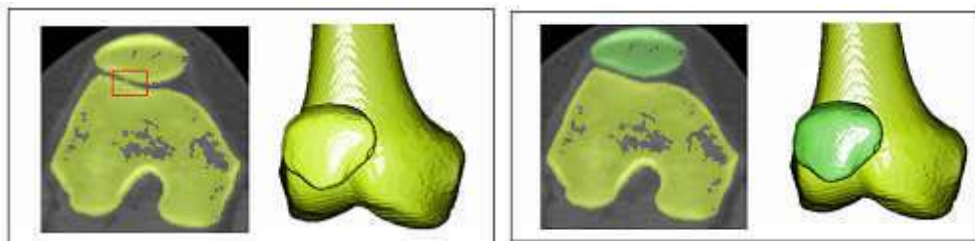Tab. 1: The DICOM information of five lower limbs in Figure 11.

Fig. 12: Critical initial threshold for separating the tibia, (a) T_i=163, all regions are still combined together, (b) T_i=164, the patella is separated.

	Case1		Case2		Case3		Case4		Case5		
	L	R	L	R	L	R	L	R	L	R	Avg.
Patella	164	152	115	116	215	213	100	102	147	182	151
Tibia	250	285	425	342	266	313	203	169	382	273	291
Fibula	312	293	425	274	305	260	176	142	382	273	284
Femur	335	312	237	242	303	299	282	297	268	332	291
Ilium	351	342	336	272	528	464	442	453	434	441	402

Tab. 2: Critical thresholds for five major bones for five lower limbs.

Skeletal area	T_i
Upper limb	300~400
Lower limb	300~400
Ilium	400~500
Feet	400~600
Spine	600~800

Tab. 3: Initial threshold T_i used in the proposed method for different area of the skeletal structures.

Next, the analysis for T_t is as follows. On each slice of the same bone, an average threshold T_{ti} along its 2D contour is evaluated using the algorithm in Section 2.2. Figures 13(a) and (b) depict the distributions of T_{ti} in terms of the slice number for the femur and tibia, respectively. The plots indicate that the thresholds near the long bone area are larger than those of the joint area. If one chooses the value near the long bone area as the target threshold T_t, the bones near the joint area may be grown incompletely (e.g., T_t=260 in Figure 13(a)). On the contrary, if one chooses the value near the valley of the joint area only, the long bone area may be over grown (e.g., T_t=110 in Figure 13(a)). In general, incomplete growing occurs more frequently than over growing and is more troublesome. Therefore, the optimal target threshold T_t for a bone is determined by averaging the first several portions and the last several portions of T_{ti} on the distribution plot.

Figure 14 depicts the procedure for evaluating the optimal target threshold T_t for each bone. First, initial bone segmentation is implemented to obtain the initial region of each bone, where T_i is determined in Table 2. Next, multiple regions growing is implemented with a target threshold of 140 to ensure that all regions are over expanded. Then, each region is filled and expanded to yield a solid region which covers the surface boundary of the bone. The boundary detection algorithm described in Section 2.2 is then implemented to extract the surface boundary. A T_{ti} on each slice of the surface boundary can then be evaluated. Finally, choose appropriate portions of T_{ti} and average them to yield the optimal target threshold T_t of the bone considered. Here the first one third and the last one third of T_{ti} on each distribution plot are employed to determine T_t.

Table 4 lists the optimal target thresholds T_t for five major bones and five lower limbs in Figure 11 by means of the above procedure. The results indicate that T_t for the left bone and the right bone of the same patient are similar (the maximum difference is 10), indicating that the same CT displays similar gray values on the left and right bones of the same patient. On the contrary, for cases 1, 2 and 3, where the same CT morality is employed on different patients, the maximum difference is increased to 35, indicating that T_t may change slightly patient by patient. The maximum difference between case 1 and case 4 is increased to 60, owing to the variation of the CT morality. The maximum difference

between case 1 and case 5 is increased as high as 74. This occurs because the contrast medium is applied in case 5.
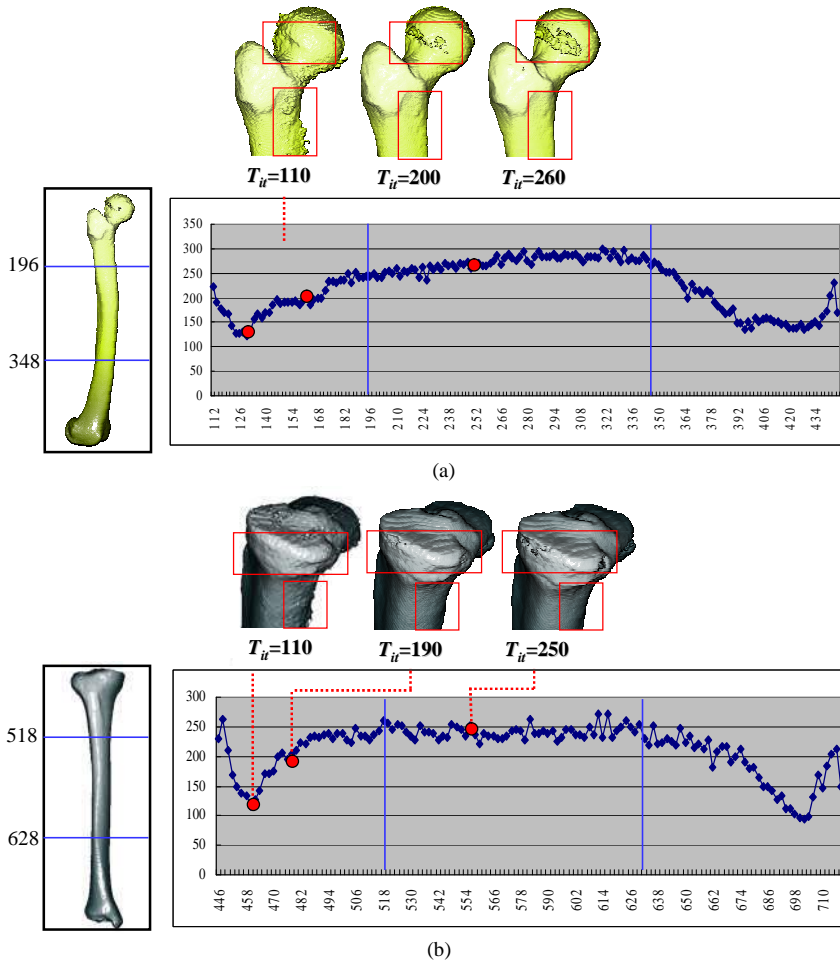

Fig. 13: Distribution of average target threshold T_{it} on two bones, (a) femur and (b) tibia.

Figure 15 depicts all bones segmented for the five lower limbs, where the T_t employed on each bone is listed in Table 4. It is noted that each color represents an isolated bone region, in which the joints of all bones are accurately separated. Each of the regions can be manipulated individually, such as in the output of a set of triangular meshes for biomedical applications. The optimal target thresholds T_t shown in Table 4 for various bones are generally smaller than the range of 180~220, which is commonly chosen for constant thresholding. The advantage of multiple-level T_t for different bone regions is illustrated in Figure 16. In general, if a constant threshold is employed, e.g. T_t=200 for all bones, substantial defects are observed on most joints (left plots in Figure 16). However, after multiple-level T_t is employed, where each bone has its own T_t, the incomplete growing problem on the joints can be improved significantly (right plots in Figure 16).
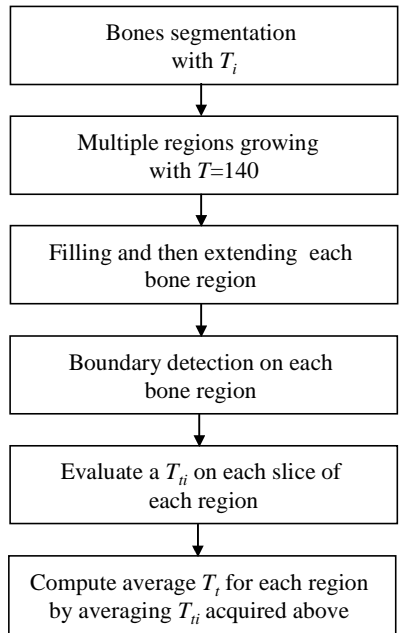
Bones segmentation
with T_i

Multiple regions growing
with T=140

Filling and then extending each
bone region

Boundary detection on each
bone region

Evaluate a T_{ti} on each slice of
each region

Compute average T_t for each region
by averaging T_{ti} acquired above

Fig. 14: Flowchart of evaluating the target threshold T_t for each bone region.

Case 1   Case 2   Case 3   Case 4   Case 5
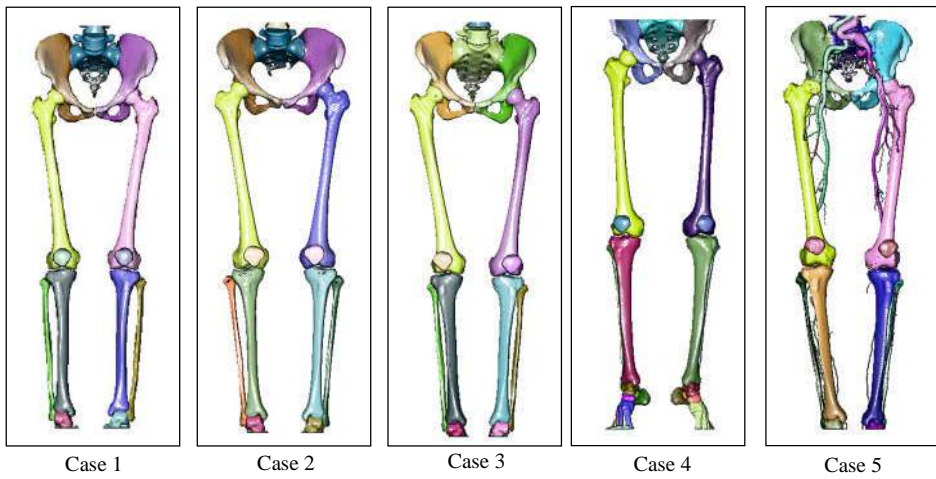
Fig. 15: Segmentation results for the five lower limbs in Figure 11.

	Case1		Case2		Case3		Case4		Case5	
	L	R	L	R	L	R	L	R	L	R
Patella	145	141	147	141	164	167	162	176	119	112
Tibia	187	175	152	158	172	162	127	127	114	116
Fibula	190	189	180	178	189	182	161	161	118	115

Femur	188	185	164	164	183	182	138	141	112	101
Ilium	142	144	135	135	135	148	142	143	113	113

Tab. 4: The result of target threshold T_t for different area of skeletal structures.
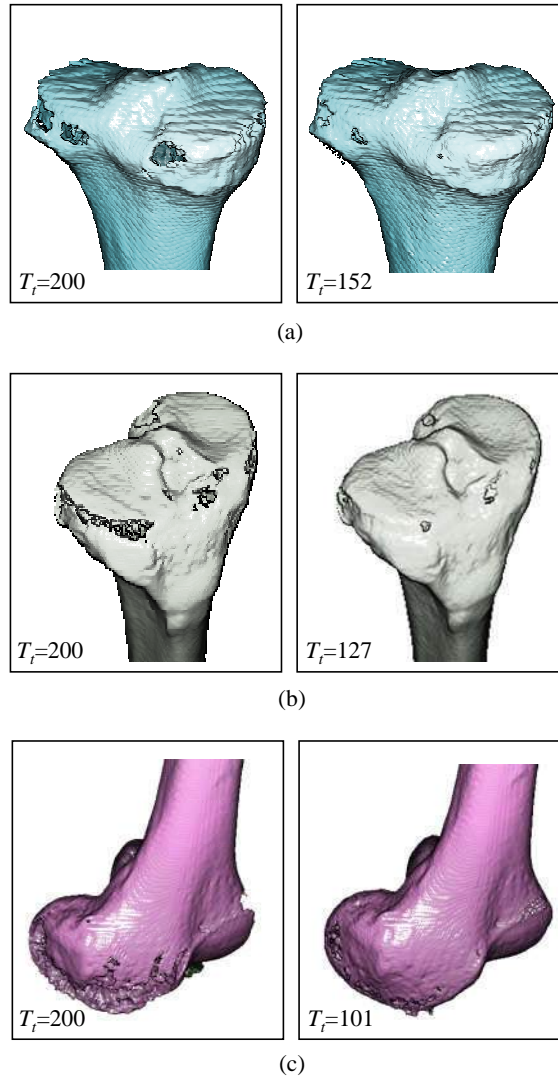

(a)

(b)

(c)

Fig. 16: A comparison of constant threshold with multiple level thresholds, (a) left tibia in Case 2, (b) left tibia in Case 4, and (c) right femur in Case 5.

Based on our experiences, the proposed algorithm works satisfactorily for normal bones as there is always a layer of cartilage between two separated bones. Although all bones may not be extracted completely with the proposed region growing algorithm, the employment of region re-segmentation and region re-combination enables the correction of incomplete segmentation and over segmentation, respectively. The processing time required for the overall process is more efficient than that of most commercial software, in which the segmentation is performed slice by slice. However, for the

segmentation of fractured bones, the fractured lines or fragments may not be recognized accurately because the transition of the gray values may not be significant on some regions of adjacent fragments. In Figure 17(a), a pelvis is broken into several pieces on the right ilium and the sacrum. Figure 17(b) depicts the segmented results, in which the regions that are not segmented accurately are expanded and displayed. The reason that they cannot be segmented correctly is because the fragments are partially connected or compressed. A manual operation is necessary to segment these regions.
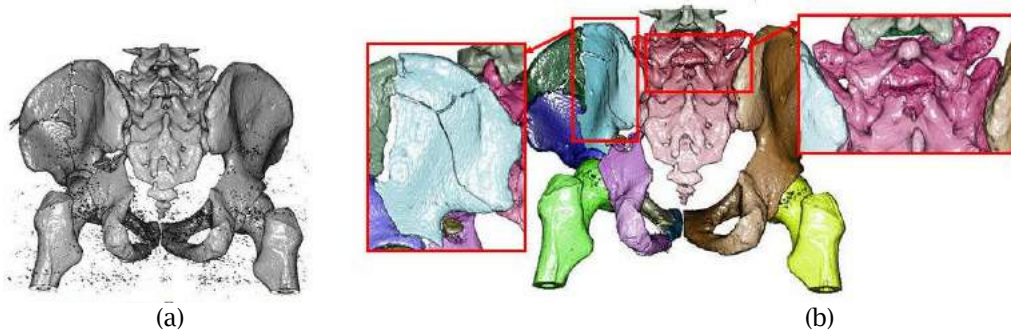

(a)   (b)

Fig. 17: A fractured pelvis not segmented correctly, (a) before segmentation, (b) after segmentation.

4   CONCLUSION

The purpose of this study is to present a method for multiple bone segmentation from CT images. It has the following features. First, a seed-region growing algorithm is developed for initial growing of the bone regions. The aim is to find an initial region for each bone of interest. A user's interface is provided so that the initial regions are displayed right after the initial threshold is specified. Second, multiple region growing is proposed to grow all regions simultaneously. Each front of the region is grown to an intermediate target threshold in each iterative cycle, which can ensure that all fronts are moved to the surface boundary at the same speed. With this strategy, overflow owing to irregular speed in region growing can be eliminated. Third, when a constant threshold is employed for all bones, undoubtedly, some of the regions will not be grown correctly. A procedure is provided to evaluate a target threshold for each region, enabling each region to be grown accurately and completely. Finally, a post-processing process including region re-combination and re-segmentation is presented to cope with all kinds of situations on CT images. The proposed method is not only suitable for lower limbs, but can also be applied for other skeletal structures. However, the optimal target threshold must be re-evaluated for different skeletal structures

REFERENCES

[1]   Palon, N. R.: Minimum Cross-Entropy Thresholding, Pattern Recognit, 29(4), 1996, 575-580. DOI:10.1016/0031-3203(95)00111-5
[2]   Brink, A. D.; Pendock, M. E.: Minimum Cross-Entropy Threshold Selection, Pattern Recognit, 29(1), 1996, 179-188. DOI:10.1016/0031-3203(95)00066-6
[3]   Otsu, N.: A Threshold Selection Method from Gray-Level Histograms, IEEE Trans Sys Man and Cyber, 9(1), 1979, 62-66. DOI:10.1109/TSMC.1979.4310076
[4]   Asano, T.; Yokoya, N.: Image Segmentation Schema for Low-Level Computer Vision, Pattern Recognit, 14(1-6), 1981, 267-273.
[5]   Revol-Muller, C.; Peyrin, F.; Carrillon, Y.; Odet, C.: Automated 3D Region Growing Algorithm Based on an Assessment Function, Pattern Recognit Lett., 23(1-3), 2002, 137-150. DOI:10.1016/S0167-8655(01)00116-7
[6]   Yin, P. Y.: Multilevel Minimum Cross Entropy Threshold Selection Based on Particle Swarm Optimization, Appl Math Comput, 184(2), 2007, 503-513. DOI:10.1016/j.amc.2006.06.057
[7]   Liao. P. S.; Chen, T. S.; Chung, P.C.: A Fast Algorithm for Multilevel Thresholding, J Inform Sci Eng, 17, 2001, 713-727.

[8] Cheriet, M.; Said, J. N.; Suen, C. Y.: A Recursive Thresholding Technique for Image Segmentation, IEEE Trans Image Process, 7(6), 1998, 918-921. DOI:10.1109/83.679444

[9] Adams, R.; Bischof, L.: Seeded Region Growing, IEEE Trans Pattern Anal Mach Intell, 16(6), 1994, 641-647. DOI:10.1109/34.295913

[10] Lin, Z.; Jin, J.; Talbot, H.: Unseeded Region Growing for 3D Image Segmentation, ACM International Conference Proceeding Series, Sydney, Australia, 2000

[11] Justice, R. K.; Stokely, E. M.; Strobel, J. S.; Ideker, R. E.; Smith, W. M.: Medical image segmentation using 3D seeded region growing, Proceedings of the SPIE Symposium on Medical Imaging, Newport Beach, California, 1997.

[12] Sekiguchi, H.; Sano, K.: Interactive 3-Dimensional Segmentation Method Based on Region Growing Method, Syst Comput Jpn. 25(1), 1994, 88-97. DOI:10.1002/scj.4690250108

[13] Hojjatoleslami, S. A.; Kittler, J.: Region Growing: A New Approach, IEEE Trans Image Process, 7(7), 1998, 1079-1084. DOI:10.1109/83.701170

[14] Pohle, R.; Toennies, K. D.: A New Approach for Model-Based Adaptive Region Growing in Medical Image Analysis, Proceedings of the 9th International Conference on Computer Analysis of Images and Patterns. Berlin, 2001.

[15] Kwan, F. Y.; Cheung, K. C.; Gibson, I.: Automatic Extraction of Bone boundaries from CT Scans Using an Intelligence-based Approach, Proceedings of the 15th International Conference on Pattern Recognition,Washington, DC, USA, 2000.

[16] Kang, Y.; Engelke, K.; Kalender, W. A.: A New Accurate and Precise 3-D Segmentation Method for Skeletal Structures in Volumetric CT Data, IEEE Trans Med Imaging, 22(5), 2003, 586-598. DOI:10.1109/TMI.2003.812265

[17] Wang, L. I.; Greenspan, M.; Ellis, R.: Validation of Bone Segmentation and Improved 3-D Registration Using Contour Coherency in CT Data, IEEE Trans Med Imaging, 25(3), 2006, 324-334. DOI:10.1109/TMI.2005.863834

[18] Descoteaux, M.; Audette, M.; Chinzei, K.; Siddiqi, K.: Bone Enhancement Filtering: Application to Sinus Bone Segmentation and Simulation of Pituitary Surgery, Compute Aided Surg, 11(5), 2006, 247-255. DOI:10.1080/10929080601017212

[19] Zoroofi, R. A.; Sato, Y.; Sasama, T.; Nishii, T.; Sugano, N.; Yonenobu, K.; Yoshikawa, H.; Ochi, T.; Tamura, S.: Automated Segmentation of Acetabulum and Femoral Head From 3-D CT Images, IEEE Trans Inf Technol Biomed, 7(4), 2003, 329-342. DOI:10.1109/TITB.2003.813791

[20] Testi, D.; Zannoni, C.; Cappello, A.; Viceconti, M.: Border-Tracing Algorithm Implementation for the Femoral Geometry Reconstruction, Comput Meth Prog Bio, 65(3), 2001, 175-182. DOI:10.1016/S0169-2607(00)00125-5

[21] Westin, C. F.; Warfield, S.; Bhalerao, Q.; Mui, L.; Richolt, J.; Kikinis, R.: Tensor Controlled Local Structure Enhancement of CT Images for Bone Segmentation, Proceedings of the First International Conference on Medical Image Computing and Computer-Assisted Intervention, London, UK, 1998.

[22] Wang, L.; Bai, J.: Threshold Selection by Clustering Gray Levels of Boundary, Pattern Recognit Lett, 24(12), 2003, 1983-1999. DOI:10.1016/S0167-8655(03)00037-0